

F61 Nuclear Magnetic Resonances

Abstract: The transverse component of magnetization undergoes precession at a position-dependent Larmor frequency ω_L , due to the inhomogeneity of the magnetic field. We utilized a Bruker Minispec p20 apparatus to generate pulses that alter magnetization and initiate nuclear magnetic resonance (NMR). We analyzed the detected signals to elucidate the relaxation process using the spin echo method and Carr-Purcell sequence, as well as to identify substances based on their chemical shifts. By determining the NMR signal at each position, we can reconstruct images of objects using discrete Fourier transform, a technique widely applied in medical research and treatments.

1 Introduction and Theory

Nuclei with nonzero spin possess a magnetic dipole moment, and all these spins combine to form the magnetization, which can experience torque when interacting with an external magnetic field \vec{B}_0 .

$$\vec{\tau} = \vec{M} \times \vec{B}_0 \quad (1)$$

Consequently, the transverse component of magnetization precesses around \vec{B}_0 , with the angular frequency of this precession, known as the Larmor frequency, being proportional to the static magnetic field \vec{B}_0 .

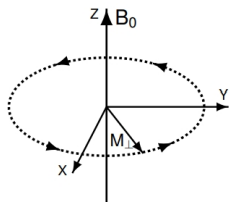


Figure 1: Precession of \vec{M}_{\perp} around \vec{B}_0 .

Due to spin-spin interaction and spin-lattice (or spin-gitter) interaction, the transverse and longitudinal components of magnetization are no longer constant and undergo a relaxation process, which can be described by the Bloch equations.

$$\frac{d\vec{M}_{\perp}(t)}{dt} = \gamma(\vec{B} \wedge \vec{M})_{\perp} - \frac{\vec{M}_{\perp}(t)}{T_2}, \quad (2)$$

$$\frac{d\vec{M}_{\parallel}(t)}{dt} = \gamma(\vec{B} \wedge \vec{M})_{\parallel} - \frac{\vec{M}_{\parallel}(t) - \vec{M}_0}{T_1}. \quad (3)$$

1.1 Relaxation

The Bloch equations assume that the time evolution of magnetization is dominated by a restor-

ing force that is linearly proportional to the deflection from equilibrium. The constant T_2 represents the spin-spin relaxation time due to interactions between magnetic dipoles, while T_1 corresponds to the spin-lattice relaxation time.

Spin-Spin relaxation

The time evolution of the transverse magnetization and longitudinal magnetization are

$$\vec{M}_{\perp}(t) = \vec{M}_{\perp}^0 e^{-\frac{t}{T_2}} \quad (4)$$

$$\vec{M}_{\parallel}(t) = \vec{M}_0(1 - 2e^{-\frac{t}{T_1}}) \quad (5)$$

- **Measurement of T_2 by spin echo method:** After a 90° pulse, the transverse magnetization begins to precess, but inhomogeneities in the magnetic field cause varying precession frequencies, leading to dephasing.

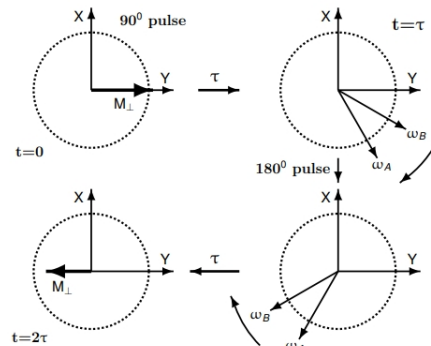


Figure 2: Visualization of spin echo method

To counteract this dephasing, a 180° pulse is applied after a time τ , reversing the phase differences. After an additional τ , the dipoles

rephase, restoring the transverse magnetization at time $t = 2\tau$ (spin echo signal).

- **Measurement of T_2 by Carr-Purcell sequence:**

The Carr-Purcell sequence enhances the spin echo method by reducing the effects of molecular diffusion and field inhomogeneities. It accomplishes this by applying a series of 180° pulses at regular intervals, which repeatedly restores phase coherence in the system.

Spin-lattice relaxation T_1

A 180° pulse initially aligns the magnetization antiparallel to the external field, and its recovery is observed over time. Subsequently, a 90° pulse is applied to convert this magnetization into a transverse signal that can be detected. By varying the time between the pulses and measuring the resulting signal, the longitudinal relaxation time T_1 can be determined.

1.2 Chemical shift

The Larmor frequency of protons is influenced by both the external magnetic field and the shielding effect of electron orbitals. This shielding, characterized by a factor σ , reduces the effective magnetic field experienced by the protons, thereby altering their Larmor frequency.

$$\omega'_L = \omega_L(1 - \sigma) \quad (6)$$

By measuring this shifted frequency and comparing it to that of a reference substance such as Tetra-Methyl-Silane, the shielding factor can be determined, which allows for the identification of substances based on their chemical shift δ_i .

$$\delta_i = \sigma_i - \sigma_{\text{TMS}} \quad (7)$$

1.3 Imaging with NMR

One-dimensional NMR imaging utilizes gradient fields superimposed on a static magnetic field to encode spatial information. Two primary methods are used for this purpose: frequency coding and phase coding. Frequency coding varies the Larmor frequency with position to facilitate signal analysis, while phase coding changes the gradient field over time to alter the phase of the signal and requires multiple sequences.

Two-dimensional NMR imaging selects a slice using a gradient field and a sinc pulse, whose Fourier transform produces a square wave signal. This allows us to easily analyze and justify the signal within our selected frequency interval. The NMR signal captures then spatial information within the slice using phase and frequency coding. The image is created by applying a two-dimensional Fourier transformation to the data.

2 Measurements

The measurements for the first two parts were conducted using a Bruker Minispec p20 apparatus, while the third part was measured using a newer Bruker Minispec mq7.5 model. Before beginning the relaxation time measurements, Puls I and Puls II must be defined as 90° and 180° pulses, respectively, in periodic mode. To achieve this, increase the pulse duration of Puls I until its output intensity on the oscilloscope is minimized, and then repeat the procedure for Puls II until its intensity is maximized. To vary the working frequency, we adjust the magnetic fringe field inside the frame by moving the iron screws within the p20 magnet to change the magnetic field configuration, so that the magnetic field in the gap can be precisely tuned.

2.1 Part I: Relaxation time

To measure the relaxation time T_2 using the spin echo and Carr-Purcell sequences, as well as the relaxation time T_1 for both Gd500 and Gd600 samples, we utilize the computational program *LabVIEW*. In the frequency domain, the signal within the spin echo zoom range forms an approximate Gaussian profile centered near the working frequency $v_w = 1\text{kHz}$. The signal strength is calculated by summing the bin contents within this profile, and the signal-to-noise ratio is improved by averaging multiple measurements. The measurements are conducted for different τ values, with the resulting data points fitted using a function defined by Eq.(4).

For the Carr-Purcell sequence, the averages over ten measurements are displayed along with the associated error, fitted by the same equation above, but only for a single τ value. However, for each sample, the time interval between the two pulses in the sequence only needs to be specified once.

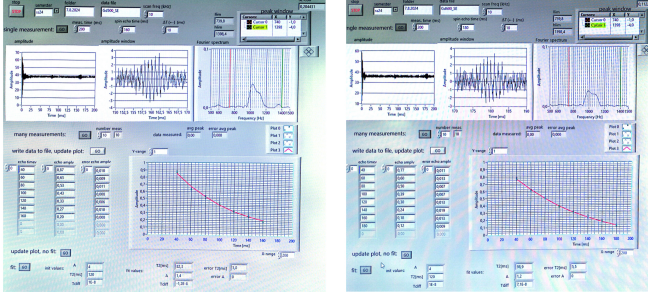


Figure 3: Spin echo method for T_2 measurement: left Gd500, right Gd600

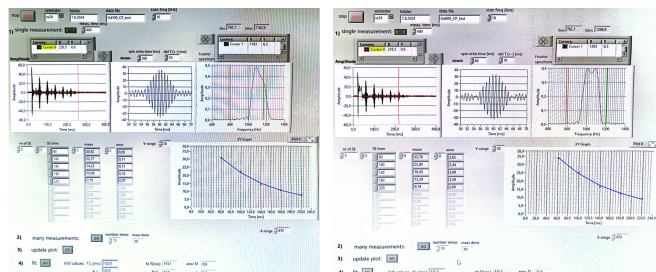


Figure 4: Carr-Purcell sequence method for T_2 measurement: left Gd500, right Gd600

The measurement of the T_1 relaxation time is done by an another application of *LabVIEW* follows the same structure as the one for the T_2 measurement by the spin echo method, except that the fitting routine is now defined by eq. (5)

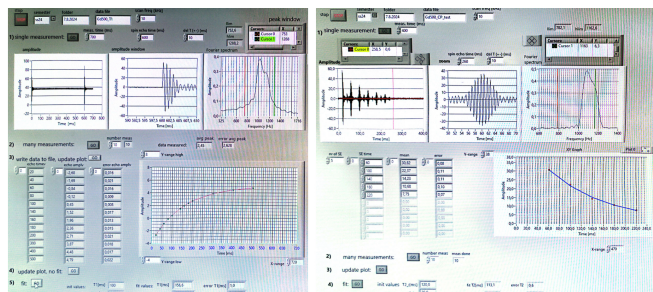


Figure 5: T_1 measurement: left Gd500, right Gd600

All measurements along with their associated errors are provided in the table below:

Measurements [ms]	Gd500	Gd600
Spin echo T_2	82.3 ± 3.8	98.9 ± 5.5
Carr-Purcell sequence T_2	113.1 ± 0.6	118.5 ± 22.4
T_1 measurement	156.6 ± 1.0	113.1 ± 0.6

Table 1: Relaxation time for different samples

The transverse relaxation times (T_2) measured using both methods are consistently shorter than the longitudinal relaxation times (T_1). The decay of transverse magnetization leads to the creation of longitudinal components, which can be influenced by interactions between nuclear spins and their surroundings, particularly due to the thermal motion of the surrounding molecules. Additionally, spin-spin interactions affect the transverse component. As a result, transverse magnetization changes more rapidly than longitudinal magnetization.

Compared to the Carr-Purcell method, the relaxation time determined by the spin echo method is significantly shorter. The spin echo method faces limitations at large 2τ values, where molecular diffusion and field inhomogeneities can lead to partial coherence—resulting in different average Larmor frequencies during the intervals $0 < t < \tau$ and $\tau < t < 2\tau$ and reduced signal strength, which lowers the observed T_2 . In contrast, the Carr-Purcell sequence mitigates the effects of molecular diffusion and field inhomogeneities, thereby minimizing the limitations of the spin echo method.

The relaxation times vary depending on the samples. Gd500, with its higher concentration, allows for more efficient energy loss through precession due to spin-spin and spin-lattice interactions. The greater the restriction on molecular mobility in a material, the shorter the T_2 time. In simple liquids like water or acetone, the T_2 time is roughly equal to the T_1 time and can be several seconds long, whereas in solids, it is typically on the order of tens of microseconds.¹

In this experiment, we have neglected systematic errors, such as thermal noise and frequency instabilities, to simplify the measurement process. The resulting error is primarily influenced by statistical uncertainty during the fitting process, particularly for the Carr-Purcell measurements with Gd600. However, this can be mitigated by conducting additional measurement series or by increasing the number of averages in the program.

¹Reference: Wikipedia NMR Relaxation

2.2 Part II: Chemical Shift

Due to the unique nature of the chemical shifts for different functional groups, it is possible to identify the substances by analyzing the position of peaks in the five samples.

toluol	$\text{CH}_3 - \text{C}_6\text{H}_5$
p-xylol	$\text{CH}_3 - \text{C}_6\text{H}_3(\text{CH}_3)_2$
acetic acid	$\text{CH}_3 - \text{COOH}$
fluoroacetone	$\text{FCH}_2 - \text{CO} - \text{CH}_3$
fluoroacetonitrile	$\text{FCH}_2 - \text{CN}$

The NMR signal of the probe is measured, and its discrete Fourier transform is calculated in steps of 2 Hz and displayed in the frequency domain.

The Larmor frequency of the reference substance TMS can be identified by comparing the measurement of the probe with that of the probe plus the reference. Evaluating the Larmor frequency ω_i relative to the reference allows for the determination of the chemical shift δ_i , as expressed in equation (7). Using the measured chemical shifts δ_i , we can identify the five substances shown above by comparing them with the information provided in the following diagram.

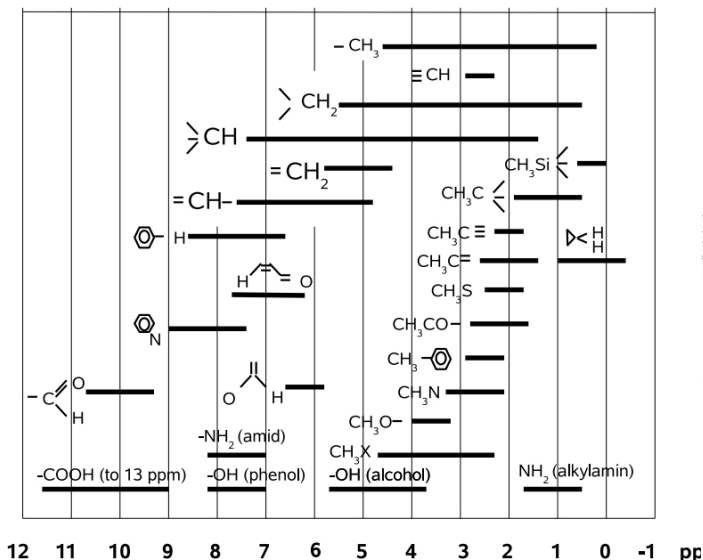
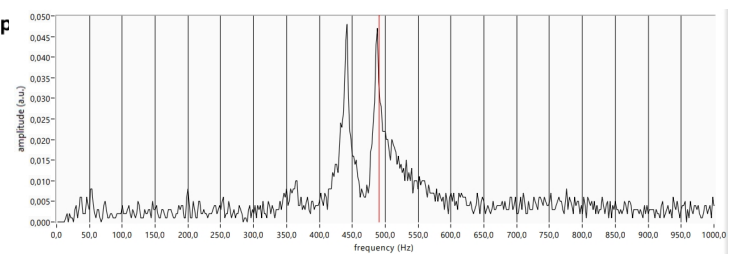
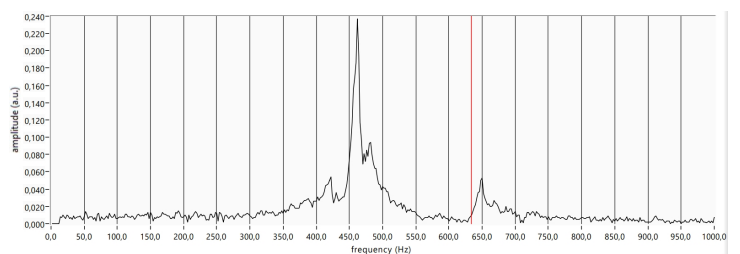
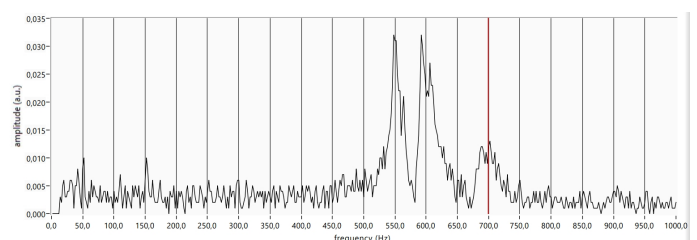
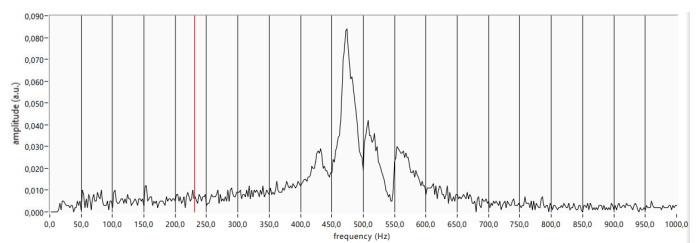


Figure 6: Chemical shifts δ_i of compounds relative to TMS

The NMR signal obtained after applying the low-pass filter is trigonometric, with its Fourier

transform theoretically representing a delta function — a very narrow peak. However, due to the spatial extent of the sample and the inhomogeneity of the magnetic field, different parts of the stationary sample experience varying Larmor frequencies. This variation causes the intensity profile within the frequency interval to appear Gaussian, thereby reducing accuracy. To compensate for spatial inhomogeneity, the sample is rotated. By rotating, the sample traverses different regions of the magnetic field, averaging out these variations over time.



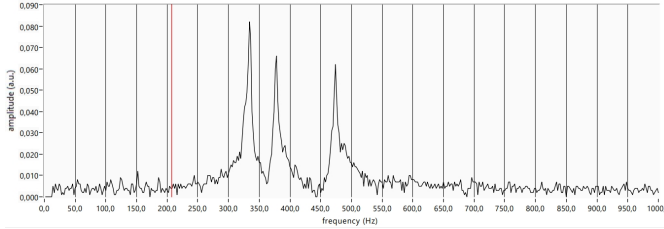


Figure 7: Spectrum von A+, B+, C+, D+ und E+

Peak [ppm]	A+	B+	C	C+	D
P1	13.0	12.3		16.7	
P2	15.3	14.8	19.2	18.9	15.6
P3	17.0	19.5	28.8	28.3	17.9
P4	20.3				

Peak [ppm]	D+	E	E+
P1	9.3		13.0
P2	13.3	16.9	15.3
P3	15.8	21.9	20.1
P4			

Table 2: Position of Peaks in the Frequency Domain. The label "+" indicates that the reference substance TMS is included in the probe. Since the spectrum of TMS is simple and consistently appears as the first peak, P1 represents the TMS peak and is recorded only for samples marked with "+".

Then we get the chemical shifts in the following table.

	A+	B+	C+	D+	E+
δ_i [ppm]	2.3 4 7.3	2.5 4.7	2.2 9.4	4 2.5	2.3 4.8

Due to the largest shift observed in C+, it must contain a carboxyl group, indicating that C is **acetic acid**. B+ and E+ exhibit nearly identical chemical shifts, suggesting they contain methyl and benzyl groups. Since toluene and p-xylene have similar chemical shifts, B and E must be these substances. In the spectrum of B+, the intensity ratio of the second and third peaks is approximately two, whereas in E+ the intensity of peaks are nearly equal. This suggests that E is toluene, as toluene contains equal amounts of methyl and benzyl groups.

Samples A and D display similar chemical shifts for the first two peaks, which can be attributed to

the splitting of the $-CH_2-$ group caused by the nuclear spins of fluorine (F) and hydrogen (H). Carbon (C) and oxygen (O) do not contribute to the spectrum, as they lack nuclear spins. Although nitrogen (N) has a nuclear spin, its resonance is not excited due to its low intrinsic frequency. This explains why fluoroacetonitrile exhibits two chemical shifts, while fluoroacetone shows three peaks.

A	fluoroacetone
B	p-xylol
C	acetic acid

D	fluoroacetonitril
E	toluol

Table 3: substance identification

Sample A (fluoroacetone) exhibited a chemical shift of 7.3 for the $-CH_3$ group, rather than the expected 4 to 5. This deviation may be attributed to the partial oxidation of the $-CO-$ group into aldehydes or carboxyl groups, which typically show higher chemical shifts.

2.3 Part III: Imaging with NMR

In this study, we investigated both one-dimensional and two-dimensional imaging using the Bruker Minispec mq7.5. For the one-dimensional measurements, we imaged the following objects within a glass tube in the vertical direction: 15 mm of oil, 50 mm of oil, and a mixture of Teflon and oil. We provide the plot below this paragraph.

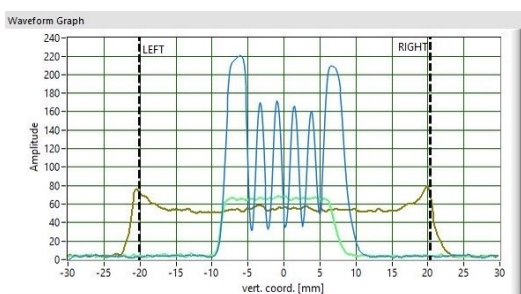


Figure 8: Experimental results for the 1-D imaging.

The green, yellow, and blue lines represent 15mm of oil, 50mm of oil, and the mixture, respectively. The curve for oil is flat due to its geometric homogeneity, which extends to the uniformity of the magnetic field. The change in the shape of the box signal for 50mm of oil suggests that the imaging range is adjustable due to the

nonlinearity of the gradient field. It is necessary to position the probe between 15mm and 50mm to obtain a high-quality image. The curve for the mixture appears periodic, with minima corresponding to the regions where Teflon does not produce an NMR signal. The peaks at the center of the curve are narrower compared to those at the left and right ends, due to the varying layer thicknesses of oil and Teflon.

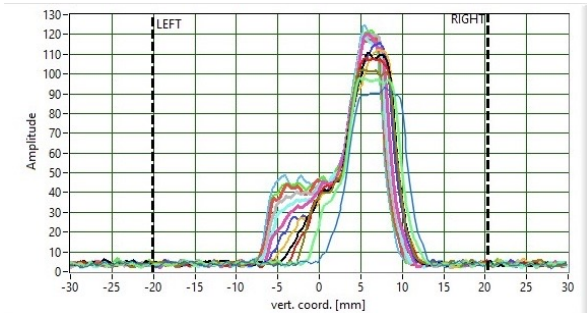


Figure 9: Diffusion experiment.

Next, we used an empty glass tube, filled it with approximately 15 mm of sand, and added 4 mm of oil on top. The signal curves evolved over time until they stabilized. We then compiled the diagrams to illustrate these changes. However, the diffusion equation for constant diffusion coefficients ²

$$\frac{\partial C(x, t)}{\partial t} = D \frac{\partial^2 C(x, t)}{\partial x^2}, \quad (8)$$

indicates that the diffusion curve should be concave. Therefore, the absence of such a curvature suggests that no diffusion is present.

In the final step, we will utilize the two-dimensional discrete Fourier transform on each selected slice to image the extended object in 3D. By using a sinc pulse with a frequency range selectively tuned for slice excitation, we can detect the NMR signals and display the resulting image in our program. Below is an image of a penut.

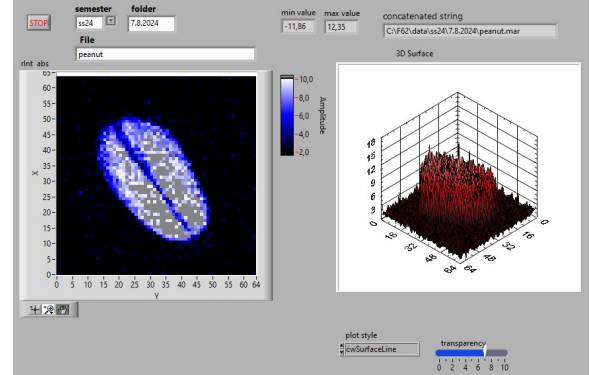


Figure 10: Display the imaging of a penut in vertical direction.

It is evident that some areas are dark while others are bright. This variation is primarily due to the differences in sensitivity of oil and water to the NMR signal. Additionally, concentration plays a role: a smaller or more dilute sample will produce a weaker signal, while increasing the sample concentration proportionally enhances the signal strength.

Our observations underscore the broad applications of NMR beyond direct observation. For instance, NMR can precisely measure tumor sizes through detailed imaging of body tissues. Additionally, it proves valuable in surface quality control, exemplified by handheld devices used to inspect the near-surface volume of car tires during production. Future advancements may focus on enhancing the sensitivity of NMR devices, as current limitations arise from magnetic field inhomogeneities. Such improvements could lead to the development of more effective magnetic field generators and facilitate further experimentation.

Reference

- [1] R. Schicker, *Nuclear Magnetic Resonance F61/F62*, Manual 3.0, march 4, 2021 <https://www.physi.uni-heidelberg.de/Einrichtungen/FP/anleitungen/F61.pdf>.
- [2] Uni DUE, 3. Theoretische Grundlagen 3.1 Spin - Gitter Relaxation, https://duepublico2.uni-due.de/servlets/MCRFileNodeServlet/duepublico_derivate_00005491/3Theorie.pdf

²Diffusion equation from Wikipedia <https://de.wikipedia.org/wiki/Diffusion>